Coordination Polymers of Copper(I) Halides

Peter M. Graham and Robert D. Pike*

Department of Chemistry, College of William and Mary, Williamsburg, Virginia 23187

Michal Sabat

Department of Chemistry, University of Virginia, Charlottesville, Virginia 22904

Rosa D. Bailey and William T. Pennington

Department of Chemistry, Clemson University, Clemson, South Carolina 29634

Received May 19, 2000

A total of 21 complexes of CuX (X = Cl, Br, I) with bridging ligand (B = 4,4′-dipyridyl (Bpy), pyrazine (Pyz), quinoxaline (Quin), phenazine (Phz), 1,4-diazabicyclo[2.2.2]octane (DABCO), and hexamethylenetetramine (HMTA)) have been synthesized. The products show two stoichiometries: [CuXB] (type **1**) and [$(CuX)_2$B] (type **2**). Both types can be obtained for B = Bpy, depending on the conditions of preparation. In these cases, the type **2** stoichiometry is the kinetic product. Type **2** complexes only are found for B = Pyz (X = I), Quin, Phz, DABCO, and HMTA. Type **1** complexes form for Pyz (X = Cl, Br). Thermogravimetic analyses of the complexes reveal the general decomposition trend: **1** → **2** → [$(CuX)_2B_{1/2}$] → CuX. The X-ray crystal structure of [CuBr(Pyz)] (type **1**) features copper atoms bridged by Br and Pyz, forming 2D sheets of fused rectangular $Cu_4Br_2(Pyz)_2$ units. The X-ray structure of [$(CuI)_2$(Quin)] (type **2**) shows 2D layers composed of $[Cu_2I_2]_\infty$ "stair step" chains which are cross-linked by Quin ligands. A total of 16 complexes of CuXL (L = $P(OPh)_3$) with bridging ligand (B = those above and 1,4-dimethylpiperazine (DMP)) have also been prepared. All of these products, except those of HMTA, are of type **3** formulation, [$(CuXL)_2$B]. The HMTA products have the formula [CuX(HMTA)], type **4**. Thermal decomposition of the type **3** and **4** complexes occurs with initial loss of B, L, or both. The X-ray structures of [$(CuBrL)_2$(Bpy)] and [$(CuBrL)_2$(Pyz)] (type **3**) reveal 1D chains formed from rhomboidal $(LCu)_2Br_2$ units linked by the B ligand. The type **4** structure of [CuBrL(HMTA)] is shown by X-ray to be a simple halide-bridged dimer.

Introduction

Although the fields of organic polymers and inorganic materials have been extensively explored, the study of metal−organic networks is relatively new. Coordination polymers and similar networks often form through simple self-assembly reactions of metal and ligand building blocks.[1,2] Nevertheless, it is not unusual for a single set of components to yield multiple structural types. Metal−organic networks are of potential interest in regard to their physical, electronic, catalytic, and structural (porosity, in particular) properties. The univalent group 11 metals are particularly attractive network formers, since they readily coordinate to unsaturated, bidentate nitrogen ligands as a result of the soft−soft bonding preference.[3] In addition, the combination of conjugated ligands, electron-rich metal centers, and the high degree of covalency inherent in soft−soft bonding can produce low-energy electronic interactions between metal centers and ligands. Interesting optical or electronic properties can result.[4−6]

When copper(I) halides (CuX) are combined with monodentate ligands (L), halide bridging produces a wide array of oligomeric structural types, as exemplified in Chart 1. Previous results have shown that the ligation mode of the halide centers (triply bridging, bridging, or terminal) is at least partially controlled by steric considerations. Thus, examples are known for monomeric,[7] square (rhomboid) dimeric,[8] cubane tetrameric,[8b,9−11] zigzag polymeric,[8a,8b,12] and "stair step" oligomeric[8a,13] structures. The common motifs in these oligomeric complexes

(1) Manners, I. *Angew. Chem., Int. Ed. Engl.* **1996**, *35*, 1602. (b) Yaghi, O. M.; Li, H.; Davis, C.; Richardson, D.; Groy, T. L. *Acc. Chem. Res.* **1998**, *31*, 474. (c) Batten, S.; Robson, R. *Angew. Chem., Int. Ed. Engl.* **1998**, *37*, 1461.

(2) Kingsborough, R. P.; Swager, T. M. *Prog. Inorg. Chem.* **1999**, *48*, 123.

(3) Munakata, M.; Wu, L. P.; Kuroda-Sowa, T. *Bull. Chem. Soc. Jpn.* **1997**, *70*, 1727. (b) Munakata, M.; Wu, L. P.; Kuroda-Sowa, T. *Adv. Inorg. Chem.* **1999**, *46*, 173 and references therein.

(4) Yam, V. W.-W.; Lo, K. K.-W. *J. Chem. Soc., Dalton Trans.* **1995**, 499. (b) Waterland, M. R.; Flood, A.; Gordon, K. C. *J. Chem. Soc., Dalton Trans.* **2000**, 121. (c) Chowdhury, S.; Patra, G. K.; Drew, M. G. B.; Chattopadhyay, N.; Datta, D. *J. Chem. Soc., Dalton Trans.* **2000**, 235.

(5) Henary, M.; Wootton, J. L.; Khan, S. I.; Zink, J. I. *Inorg. Chem.* **1997**, *36*, 796.

(6) Gan, X.; Munakata, M.; Kuroda-Sowa, T.; Maekawa, M. *Bull. Chem. Soc. Jpn.* **1994**, *67*, 3009. (b) Gan, X.; Munakata, M.; Kuroda-Sowa, T.; Maekawa, M.; Misaki, Y. *Polyhedron* **1995**, *14*, 1343. (c) Munakata, M.; Kuroda-Sowa, T.; Maekawa, M.; Hirota, A.; Kitagawa, S. *Inorg. Chem.* **1995**, *34*, 2705.

(7) Davis, P. H.; Belford, R. L.; Paul, I. C. *Inorg. Chem.* **1973**, *12*, 213. (b) Dyason, J. C.; Healy, P. C.; Pakawatchai, C.; Patrick, V. A.; White, A. H. *Inorg. Chem.* **1985**, *24*, 1957. (c) Alyea, E. C.; Ferguson, G.; Malito, J.; Ruhl, B. L. *Inorg. Chem.* **1985**, *24*, 3720.

10.1021/ic0005341 CCC: $19.00 © 2000 American Chemical Society
Published on Web 10/11/2000

Chart 1

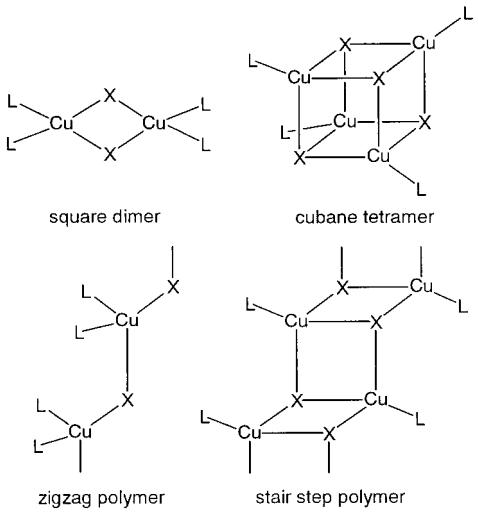

are the cyclic Cu_2X_2 dimer and the $(CuX)_\infty$ zigzag polymer, which may be regarded as a ring-opened form of the dimer.

Known combinations of copper(I) halide with bidentate bridging (B) ligands have resulted in 1D chain or 2D sheet networks, usually through the linking of Cu_2X_2 rings or $(CuX)_\infty$ chains by the larger B ligands. Several structural types have been identified through X-ray crystallography (see Chart 2). Type **1a** constitutes a sheetlike network having 1:1 CuX:B stoichiometry; it is recognized for [CuCl(4,4′-Bpy)],[14] [CuBr(3,4′-Bpy)],[15] and [CuI(dtpcp)][16] (Bpy = dipyridyl, dtpcp = 2,11-dithia[3.3]paracyclophane; see Chart 3 for a list of the ligands used in this study and their abbreviations). Although all type **1a** lattices are constructed of linked Cu_2X_2 units to form sheets of fused rings, the supramolecular structures vary. For [CuCl(Bpy)] the Cu_2Cl_2 units are shared between fused Cu_6B_6 hexagons and $(Cu_2Cl_2)_2B_2$ rectangles. However, in the case of [CuBr(3,4′-Bpy)], the $(Cu_2Br_2)_2B_2$ rectangles are linked into ladders. Another structure found for CuXB complexes is type **1b**, which consists of 2D sheets based on cross-linked $(CuX)_\infty$ chains. Such is the case for [CuBr(cnge)][17] (cnge = 1-cyanoguanidine) and [CuCl(Pyz)].[18]

Complexes having $[(CuX)_2B]$ stoichiometry are also recognized. Variants of structural type **2** have been found for $[(CuX)_2(Phz)]$ (X = Cl, Br, I).[19] Additional interchain bridging of the halides (indicated by the dashed lines in Chart 2) occurs with X = Cl and Br. As a result, copper is four-coordinate in the chloride and bromide complexes and three-coordinate in the iodide complex. The $[(CuCl)_2(Pyz)]$ structure also shows four-

Chart 2

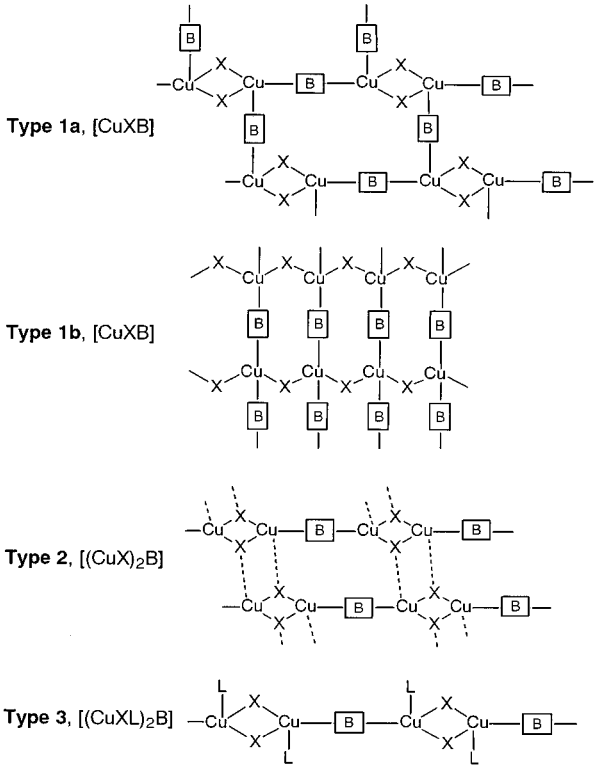

Chart 3

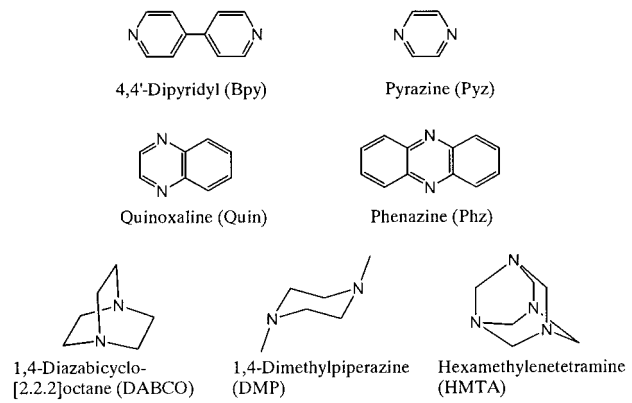

(8) Campbell, J. A.; Raston, C. L.; White, A. H. *Aust. J. Chem.* **1977**, *30*, 1937. (b) Churchill, M. R.; Rotella, R. J. *Inorg. Chem.* **1979**, *18*, 166. (c) Healy, P. C.; Pakawatchai, C.; Raston, C. L.; Skelton, B. W.; White, A. H. *J. Chem. Soc., Dalton Trans.* **1983**, 1905. (d) Healy, P. C.; Pakawatchai, C.; White, A. H. *J. Chem. Soc., Dalton Trans.* **1983**, 1917. (e) Dyason, J. C.; Engelhardt, L. M.; Healy, P. C.; White, A. H. *Aust. J. Chem.* **1984**, *37*, 2201. (f) Engelhardt, L. M.; Papasergio, R. I.; Healy, P. C.; White, A. H. *Aust. J. Chem.* **1984**, *37*, 2206. (g) Dyason, J. C.; Engelhardt, L. M.; Pakawatchai, C.; Healy, P. C.; White, A. H. *Aust. J. Chem.* **1985**, *38*, 1247. (h) Dyason, J. C.; Engelhardt, L. M.; Healy, P. C.; Pakawatchai, C.; White, A. H. *Inorg. Chem.* **1985**, *24*, 1950. (i) Rath, N. P.; Holt, E. M.; Tanimura, K. *J. Chem. Soc., Dalton Trans.* **1986**, 2303. (j) Healy, P. C.; Kildea, J. D.; White, A. H. *Aust. J. Chem.* **1989**, *42*, 2206.

(9) Pike, R. D.; Starnes, W. H., Jr.; Carpenter, G. B. *Acta Crystallogr., Sect. C* **1999**, *55*, 162.

(10) Barron, P. F.; Dyason, J. C.; Engelhardt, L. M.; Healy, P. C.; White, A. H. *Inorg. Chem.* **1984**, *23*, 3766 and references therein.

(11) Dyason, J. C.; Healy, P. C.; Engelhardt, L. M.; Pakawatchai, C.; Patrick, V. A.; Raston, C. L.; White, A. H. *J. Chem. Soc., Dalton Trans.* **1985**, 831. (b) Engelhardt, L. M.; Healy, P. C.; Kildea, J. D.; White, A. H. *Aust. J. Chem.* **1989**, *42*, 107. (c) Engelhardt, L. M.; Gotsis, S.; Healy, P. C.; Kildea, J. D.; Skelton, B. W.; White, A. H. *Aust. J. Chem.* **1989**, *42*, 149. (d) Babich, O. A.; Kokozay, V. N. *Polyhedron* **1997**, *16*, 1487.

(12) Healy, P. C.; Kildea, J. D.; Skelton, B. W.; White, A. H. *Aust. J. Chem.* **1989**, *42*, 115.

(13) Strahle, J.; Hiller, W.; Eitel, E.; Oelkrug, D. *Z. Kristallogr.* **1980**, *153*, 277. (b) Healy, P. C.; Kildea, J. D.; Skelton, B. W.; White, A. H. *Aust. J. Chem.* **1989**, *42*, 79. (c) Healy, P. C.; Kildea, J. D.; Skelton, B. W.; White, A. H. *Aust. J. Chem.* **1989**, *42*, 93. (d) Engelhardt, L. M.; Healy, P. C.; Kildea, J. D.; White, A. H. *Aust. J. Chem.* **1989**, *42*, 185 and references therein.

(14) Yaghi, O. M.; Li, G. *Angew. Chem., Int. Ed. Engl.* **1995**, *34*, 207.

(15) Fun, H.-K.; Raj, S. S. S.; Xiong, R.-G.; Zuo, J.-L.; Yu, Z.; Zhu, X.-L.; You, X.-Z. *J. Chem. Soc., Dalton Trans.* **1999**, 1711.

(16) Munakata, M.; Wu, L. P.; Kuroda-Sowa, T.; Maekawa, M.; Suenaga, Y.; Nakagawa, S. *J. Chem. Soc., Dalton Trans.* **1996**, 1525.

(17) Begley, M. J.; Eisenstein, O.; Hubberstey, P.; Jackson, S.; Russell, C. E.; Walton, P. H. *J. Chem. Soc., Dalton Trans.* **1994**, 1935.

(18) Moreno, J. M.; Suarez-Varela, J.; Colacio, E.; Avila-Roson, J. C.; Hildago, M. A.; Martin-Ramos, D. *Can. J. Chem.* **1995**, *73*, 1591.

(19) Munakata, M.; Kuroda-Sowa, T.; Maekawa, M.; Honda, A.; Kitagawa, S. *J. Chem. Soc., Dalton Trans.* **1994**, 2771.

coordination.[20] When tetradentate bridging ligands, B, are employed, the $[(CuX)_2B]$ polymers show four-coordinate copper.[6,21] Several recent papers have described the crystal structures of CuSCN,[22,23] CuNCO,[24] CuN_3,[22] and CuCN,[25] with Pyz, Bpy, and several other bridging ligands; these exhibit variations on the type **1b** motif.

The addition of a terminal (L) ligand to the CuX−B system has been shown to produce 2:2:1 CuX:L:B complexes having 1D type **3** structures. Several such polymers have been reported, including: $[(CuCl)_2(PPh_3)_2(Pyz)]$,[5] $[(CuCl)_2(PPh_3)_2(Bpy)]$,[26] $[(Cu(\mu\text{-}NO_3))_2(PPh_3)_2(Bpy)]$,[27] and $[(CuBr)_2(NCMe)_2(dtpcp)]$.[16]

In this paper, we present an extensive study of CuX−B and CuX−L−B systems (X = Cl, Br, I; L = $P(OPh)_3$; B = various bidentate, bridging nitrogen ligands; see Chart 3). In the course of the investigation, we have solved crystal structures showing both 1:1 and 2:1 stoichiometries for CuX−B and CuXL−B systems. The delicate balance between 2:1 and 1:1 complexes in the CuX−Bpy and CuX−Pyz systems was uncovered.

Experimental Section

General Methods. All syntheses were carried out under nitrogen atmosphere. Flame atomic absorption spectroscopy (AAS) was performed with a Perkin-Elmer 1100B spectrophotometer. Microanalyses for C, H, and N were carried out by Atlantic Microlab, Inc., Norcross, GA. All TGA analyses were conducted on a Shimadzu TGA-50 instrument.

Materials. All ligands were purchased from Aldrich or Acros and were used as received, except for quinoxaline, which was sublimed under reduced pressure before use. Copper(I) chloride and bromide were freshly recrystallized from aqueous HCl or HBr. Copper(I) iodide was used as received from Aldrich. The phosphite complexes $[CuCl(P(OPh)_3)]_4$ and $[CuBr(P(OPh)_3)]_4$ were prepared and purified according to literature procedures.[9,28] Ultrex nitric acid was purchased from Baker Chemical.

Preparation of $[(CuBr)_2(Quin)]$. Freshly recrystallized CuBr (0.510 g, 3.55 mmol) was dissolved in 40 mL of CH_3CN. The solution was filtered through Celite to remove traces of Cu(II) species and was stirred under nitrogen at 25 °C. A solution of quinoxaline (0.485 g, 3.73 mmol) in 10 mL of CH_3CN was added to the CuBr solution via syringe. An orange precipitate rapidly developed. After stirring of the mixture for 30 min at 25 °C, the product was collected via filtration, washed with diethyl ether, and then dried under vacuum (0.547 g, 1.31 mmol, 74%). Other type **1** and **2** complexes (see Table 1) were prepared similarly.

Preparation of $[(CuCl)_2(P(OPh)_3)_2(Pyz)]$. $[CuCl(P(OPh)_3)]_4$ (0.911 g, 0.556 mmol) and additional $P(OPh)_3$ (0.355 g, 1.14 mmol) were dissolved in 40 mL of $CHCl_3$ at 25 °C. Pyrazine (0.0913 g, 1.14 mmol) in 10 mL of $CHCl_3$ was added by use of syringe. A yellow solution resulted. Addition of an equal volume of diethyl ether, followed by cooling for several hours, resulted in the formation of a yellow crystalline solid. The product was collected via filtration, washed with diethyl ether, and then dried under vacuum (0.791 g, 0.880 mmol, 79%). Other type **3** and **4** complexes (see Table 2) were prepared similarly. Iodide complexes were prepared by using a solution mixture of CuI and $P(OPh)_3$ in CH_3CN.

Atomic Absorption Analysis. Sample stock solutions were prepared by digesting 10−13 mg of complex in about 1 mL of Ultrex HNO_3 at room temperature and then heating the mixture at about 50 °C for about 5 min. The samples were diluted to 100 mL with water. Solutions for analysis were prepared by diluting 1 or 2 mL of the stock solutions to 25 mL with water. Standards were prepared by diluting a 1000 ppm stock solution of $Cu(NO_3)_2$ to 500, 1000, 1500, 2000, and 2500 ppb in dilute nitric acid. Absorption measurements were made at 324 nm.

X-ray Diffraction Studies. The complexes were crystallized as follows. [CuBr(Pyz)]: Equal portions of 20 mM Pyz in CH_3CN and 8.0 mM CuBr in CH_3CN were combined. The colorless solution was heated to 70 °C in a sealed vial under Ar, and then cooled to 25 °C. Small red crystals formed upon standing overnight. $[(CuI)_2(Quin)]$: 0.050 mmol of Quin were dissolved into a CH_3CN solution of CuI (10 mL, 10 mM). The red suspension solution was heated to 70 °C in a sealed vial under argon for 7 days, producing red plate crystals. $[(CuBr)_2(P(OPh)_3)_2(Pyz)]$: 0.10 mmol of Pyz were rapidly dissolved into a CH_3CN solution of $[CuBr(P(OPh)_3)]_4$ (10 mL, 10 mM based on monomer). The solution was allowed to stand overnight at 25 °C, yielding yellow parallelepiped crystals. $[(CuBr)_2(P(OPh)_3)_2(Bpy)]$: Small yellow crystals were grown by diffusion of CH_3CN solutions of $[CuBr(P(OPh)_3)]_4$ (10 mM based on monomer) and Bpy (10 mM) at 10 °C through a layer of pure CH_3CN in a 5-mm i.d. tube. $[(CuBr)(P(OPh)_3)(HMTA)]$: 0.10 mmol HMTA were suspended in a CH_3CN solution of $[CuBr(P(OPh)_3]_4$ (10 mL, 10 mM based on monomer). The mixture was sealed in a vial under Ar and heated to 70 °C for 1 h, forming a solution, which was allowed to cool to 25 °C and stand overnight. Small colorless needle crystals formed. The chloro derivative of $[(CuBr)(P(OPh)_3)(HMTA)]$ was also analyzed and was found to be isomorphous with the bromo derivative.[29] However, crystals of the chloro complex were of very poor quality and gave an unacceptable refinement.

Crystals were mounted on glass fibers. For all structures except $[(CuBr)_2(P(OPh)_3)_2(Bpy)]$, all measurements were made on a Mercury CCD area detector coupled with a Rigaku AFC-8S diffractometer with graphite-monochromated Mo Kα radiation. Final cell parameters were obtained from a least-squares analysis of reflections with $I > 5\sigma(I)$. Space group determinations were made on the basis of systematic absences, a statistical analysis of intensity distribution, and the successful solution and refinement of the structure. Data were collected at a temperature of 20 ± 1 °C to a maximum 2θ value of 52.9°. Data were collected in 0.5° oscillations (in ω) with 10.0 s exposures (in two 5.0 s repeats to allow dezingering). Sweeps of data were done using ω oscillations from −90.0 to 90.0° at $\chi = 45.0°$ and $\phi = 0.0°$ and from −30.0 to 30.0° at $\chi = 45.0°$ and $\phi = 90.0°$. The crystal-to-detector distance was 26.72 mm, and the detector swing angle was 0.0°.

Data were collected and processed[30] using Crystal Clear.[31] The linear absorption coefficient for Mo Kα radiation is 10.28 mm^{-1}; an empirical absorption correction[32] resulted in acceptable transmission factors. The data were corrected for Lorentz and polarization effects. For $[(CuBr)_2(P(OPh)_3)_2(Pyz)]$ an additional correction for secondary extinction was applied ($x = 0.014(4)$).[33] The structures were solved by direct methods.[34]

(20) Kawata, S.; Kitagawa, S.; Kumagai, H.; Iwabuchi, S.; Katada, M. *Inorg. Chim. Acta* **1998**, *267*, 143.
(21) Brook, D. J. R.; Lynch, V.; Conklin, B.; Fox, M. A. *J. Am. Chem. Soc.* **1997**, *119*, 5155.
(22) Goher, M. A. S.; Mautner, F. A. *Polyhedron* **1999**, *18*, 1805.
(23) Blake, A. J.; Brooks, N. R.; Champness, N. R.; Crew, M.; Hanton, L. R.; Hubberstey, P.; Parsons, S.; Schroder, M. *J. Chem. Soc., Dalton Trans.* **1999**, 2813.
(24) Goher, M. A. S.; Mautner, F. A. *J. Chem. Soc., Dalton Trans.* **1999**, 1923.
(25) Chesnut, D. J.; Zubieta, J. *J. Chem. Soc., Chem. Commun.* **1998**, 1707. (b) Chesnut, D. J.; Kusnetzow, A.; Zubieta, J. *J. Chem. Soc., Dalton Trans.* **1998**, 4081. (c) Stocker, F. B.; Staeva, T. P.; Rienstra, C. M.; Britton, D. *Inorg. Chem.* **1999**, *38*, 984.
(26) Lu, J.; Crisci, G.; Niu, T.; Jacobson, A. J. *Inorg. Chem.* **1997**, *36*, 5140.
(27) Prest, P.-J.; Moore, J. S. *Acta Crystallogr., Sect. C* **1996**, *52*, 2176.
(28) Nishizawa, Y. *Bull. Chem. Soc. Jpn.* **1961**, *34*, 1170.
(29) Cell parameters for $[CuCl(P(OPh)_3)(HMTA)]$: $a = 12.696(1)$ Å; $b = 11.711(2)$ Å; $c = 16.933(1)$ Å; $\beta = 103.43(1)°$; $V = 2448.8(4)$ Å^3.
(30) Data Reduction: $F^2 = [\Sigma(P_i - mB_{ave})]Lp$ (P_i is the value in counts of the ith pixel, m is the number of pixels in the integration area, B_{ave} is the background average, and Lp is the Lorentz and polarization factor); $B_{ave} = \Sigma(B_j)/n$ (n is the number of pixels in the background area; B_j is the value of the jth pixel in counts); $\sigma^2(F^2_{hkl}) = [(\Sigma P_i) + m((\Sigma(B_{ave} - B_j)^2)/(n-1))]Lp \times \text{errmul} + (\text{erradd} \times F^2)^2$ (erradd = 0.00; errmul = 1.00).
(31) *Crystal Clear*; Rigaku Corp.: Tokyo, 1999.
(32) Jacobson, R. A. *REQABS*, version 1.1; Molecular Structure Corp.: The Woodlands, TX, 1998.
(33) See: Larson, A. C. In *Crystallographic Computing*; Ahmed, F. R., Hall, S. R., Huber, C. P., Eds.; Munksgaard: Copenhagen, 1970; pp 291−294.
(34) Sheldrick, G. M. *SHELXTL, Crystallographic Computing System*, Version 5.1; Bruker Analytical X-ray Systems: Madison, WI, 1997.

Table 1. Synthetic and Analytical Data for [(CuX)B] and [$(CuX)_2$B] Complexes

compd	type	yield, %	color	element	% (theory)	% (expt)
[CuCl(Bpy)]	**1**	95	brick red	Cu	24.90	25.33
[$(CuCl)_2$(Bpy)]	**2**	96	yellow	Cu	35.88	35.65
[CuBr(Bpy)]	**1**	74	red	Cu	21.21	20.76
				C	40.08	40.98
				H	2.68	2.80
				N	9.35	9.65
[$(CuBr)_2$(Bpy)]	**2**	84	yellow	Cu	28.68	28.53
				C	27.10	27.11
				H	1.82	1.83
				N	6.32	6.30
[CuI(Bpy)]	**1**	84	red-orange	Cu	18.33	19.05
				C	34.65	33.24
				H	2.33	2.27
				N	8.08	7.64
[$(CuI)_2$(Bpy)]	**2**	92	yellow	Cu	23.66	23.86
				C	22.36	22.21
				H	1.50	1.40
				N	5.22	5.09
[CuCl(Pyz)]	**1**	77	red	Cu	35.48	36.39
				C	26.83	26.49
				H	2.25	2.26
				N	15.64	15.21
[CuBr(Pyz)]	**1**	84	red	Cu	28.43	27.17
[$(CuI)_2$(Pyz)]	**2**	70	bright yellow	Cu	27.57	27.21
				C	10.42	10.78
				H	0.87	0.96
				N	6.08	6.05
[$(CuCl)_2$(Quin)]	**2**	76	red-brown	Cu	38.72	37.10
[$(CuBr)_2$(Quin)]	**2**	74	red	Cu	30.47	30.65
				C	23.04	23.06
				H	1.45	1.44
				N	6.72	6.66
[$(CuI)_2$(Quin)]	**2**	78	red	Cu	24.87	24.17
				C	18.80	18.93
				H	1.18	1.22
				N	5.48	5.41
[$(CuCl)_2$(Phz)]	**2**	66	dark brown	Cu	33.60	33.45
[$(CuBr)_2$(Phz)]	**2**	73	dark brown	Cu	27.21	27.00
[$(CuI)_2$(Phz)]	**2**	70	gold-black	Cu	19.82	20.52
				C	25.69	26.50
				H	1.44	1.47
				N	4.99	5.08
[$(CuCl)_2$(DABCO)]	**2**	82	light brown	Cu	40.97	40.03
[$(CuBr)_2$(DABCO)]	**2**	81	light brown	Cu	31.84	30.08
				C	18.06	18.39
				H	3.03	3.66
				N	7.02	7.19
[$(CuI)_2$(DABCO)]	**2**	50	off-white	Cu	25.77	26.23
				C	14.62	14.96
				H	2.45	2.46
				N	5.68	5.56
[$(CuCl)_2$(HMTA)]	**2**	67	sandy	Cu	37.58	37.41
[$(CuBr)_2$(HMTA)]	**2**	63	white	Cu	29.76	28.77
				C	16.87	17.49
				H	2.83	2.82
				N	13.12	12.76
[$(CuI)_2$(HMTA)]	**2**	66	white	Cu	24.39	24.24

Least-squares refinement of F^2 used all reflections.[35] The non-hydrogen atoms were refined anisotropically. Hydrogen atoms were located by standard difference Fourier techniques and were refined with isotropic thermal parameters. The final cycle of full-matrix least-squares refinement was based on all unique reflections and the listed number of variable parameters and converged (largest parameter shift was 0.001 times its esd) with final residual values[35] as listed in Table 4. The weighting scheme was based on counting statistics and included factors[36] to reduce statistical bias.[35] Analysis of the variance of reflections based on sin θ/λ, magnitude of F, and parity class showed no unusual trends. Structure solution, refinement, and the calculation of derived results were performed using the SHELXTL[34] package of computer programs. Neutral atom scattering factors were those of Cromer and Waber,[37] and the real and imaginary anomalous dispersion corrections were those of Cromer.[38]

(35) Least-squares refinement: weighting scheme, $w = 1/[\sigma^2(F_o^2) + (aP)^2 + bP]$ ($P = [2F_c^2 + \mathrm{MAX}(F_o^2, 0)]/3$); residuals, $R_1 = \Sigma||F_o| - |F_c||/\Sigma|F_o|$, $wR_2 = \{\Sigma[w(F_o^2 - F_c^2)^2]/\Sigma[w(F_o^2)^2]\}^{1/2}$; goodness of fit indicator, $S = \{\Sigma[w(F_o^2 - F_c^2)^2]/(n - p)\}^{1/2}$ (n = number of reflections; p = number of parameters refined).

(36) Factors: for [CuBr(Pyz)], $a = 0.0828$, $b = 0.1223$; for [$(CuI)_2$(Quin)], $a = 0.0678$, $b = 1.113$; for [$(CuBr)_2(P(OPh)_3)_2$(Pyz)], $a = 0.0287$, $b = 0.8243$; for [CuBr$(P(OPh)_3)$(HMTA)], $a = 0.0292$, $b = 0.0$.

(37) Cromer, D. T.; Waber, J. T. *International Tables for X-ray Crystallography*; The Kynoch Press: Birmingham, England, 1974; Vol. IV, Table 2.2B.

(38) Cromer, D. T. *International Tables for X-ray Crystallography*; The Kynoch Press: Birmingham, England, 1974; Vol. IV, Table 2.3.1.

Table 2. Synthetic and Analytical Data for $[(CuXL)_2B]$ and $[(CuXL)B]_2$ Complexes[a]

compd	type	yield, %	color	element	% (theory)	% (expt)
$[(CuClL)_2(Bpy)]$	**3**	78	yellow	Cu	13.03	12.83
$[(CuBrL)_2(Bpy)]$	**3**	86	yellow	Cu	11.88	12.10
				C	51.94	51.70
				H	3.60	3.70
				N	2.63	2.57
$[(CuIL)_2(Bpy)]$	**3**	92	yellow	Cu	10.98	11.10
				C	47.73	47.95
				H	3.31	3.34
				N	2.41	2.55
$[(CuClL)_2(Pyz)]$	**3**	79	yellow	Cu	14.14	14.18
				C	53.46	53.29
				H	3.81	3.85
				N	3.12	3.11
$[(CuBrL)_2(Pyz)]$	**3**	79	yellow	Cu	12.87	13.34
				C	48.65	48.54
				H	3.47	3.46
				N	2.84	2.82
$[(CuIL)_2(Pyz)]$	**3**	81	bright yellow	Cu	11.55	11.75
$[(CuClL)_2(Quin)]$	**3**	56	orange	Cu	13.40	12.81
				C	55.71	55.06
				H	3.83	3.85
				N	2.95	2.88
$[(CuBrL)_2(Quin)]$	**3**	81	orange	Cu	12.18	11.83
				C	50.93	50.26
				H	3.50	3.48
				N	2.70	2.67
$[(CuClL)_2(Phz)]$	**3**	48	red-brown	Cu	12.72	13.51
				C	57.72	55.77
				H	3.83	3.76
				N	2.80	3.21
$[(CuClL)_2(DABCO)]$	**3**	95	cream	Cu	13.65	13.68
$[(CuBrL)_2(DABCO)]$	**3**	90	white	Cu	12.39	12.43
				C	49.47	48.89
				H	4.15	4.20
				N	2.75	2.76
$[(CuIL)_2(DABCO)]$	**3**	75	white	Cu	11.41	11.45
				C	45.30	45.40
				H	3.80	3.80
				N	2.52	2.51
$[(CuClL)_2(DMP)]$	**3**	65	white	Cu	13.62	13.17
$[(CuBrL)_2(DMP)]$	**3**	77	white	Cu	12.44	12.69
				C	49.37	49.37
				H	4.34	4.39
				N	2.74	2.71
$[(CuClL)(HMTA)]_2$	**4**	91	cream	Cu	11.56	11.63
				C	52.46	52.35
				H	4.95	4.98
				N	10.20	10.29
$[(CuBrL)(HMTA)]_2$	**4**	90	white	Cu	10.64	10.75
				C	48.53	48.59
				H	4.58	4.69
				N	9.31	9.31

[a] $L = P(OPh)_3$.

For $[(CuBr)_2(P(OPh)_3)_2(Bpy)]$ all measurements were made on a Rigaku AFC-6S diffractometer with graphite-monochromated Mo Kα radiation. Cell constants and an orientation matrix for data collection, obtained from a least-squares refinement using the setting angles of 25 carefully centered reflections in the range $20.00 < 2\theta < 35.00°$, corresponded to a primitive triclinic cell. The data were collected at a temperature of -100 ± 1 °C using the $\omega-2\theta$ scan technique to a maximum 2θ of 47.0°. ω scans of several intense reflections, made prior to data collection, had an average width at half-height of 0.32° with a takeoff angle of 6.0°. Scans of $(1.47 + 0.30 \tan \theta)°$ were made at a speed of 2° min^{-1} (in ω). The weak reflections ($I < 12.0\sigma(I)$) were rescanned (maximum of 4 scans), and the counts were accumulated to ensure good counting statistics. Stationary background counts were recorded on each side of the reflection. The ratio of peak counting time to background counts was 2:1. The intensities of three representative reflections were measured every 100 reflections. No decay correction was applied. An empirical absorption correction was applied, which resulted in transmission factors ranging from 0.79 to 1.00. The data were corrected for Lorentz and polarization effects.

The structure was solved by direct methods[39] and expanded using Fourier techniques.[40] The non-hydrogen atoms were refined anisotropically. Hydrogen atoms were included but not refined. The final cycle of full-matrix least-squares refinements[41] was based on 2100 observed reflections ($I > 3.0\sigma(I)$) and 271 variable parameters. Neutral atom scattering factors were taken from Cromer and Waber.[36] Anomalous dispersion effects were included in F_{calc};[42] the values for $\Delta f'$ and $\Delta f''$ were those of Creagh and McAuley.[43] The values for the mass

(39) Altomare, A.; Burla, M. C.; Camalli, M.; Cascarano, M.; Giacovazzo, C. Guagliardi, A.; Polidori, G. *SIR92*; **1994**.
(40) DIRDIF92: Beurskens, P. T.; Admiraal, G.; Beurskens, G.; Bosman, W. P.; Garcia-Granda, S.; Gould, R. O.; Smits, J. M. M.; Smykalla, C. *The DIRDIF program system*; Technical Report of the Crystallography Laboratory, University of Nijmegen: Nijmegen, The Netherlands, 1992.
(41) Least-squares function minimized: $\Sigma w(|F_o| - |F_c|)^2$, where $w = [1/\sigma^2(F_o)] = [(4F_o^2)/(\sigma^2(F_o^2))]$; residuals, $R = \Sigma||F_o| - |F_c||/\Sigma|F_o|$ for observed data only; $R_w = \{\Sigma[w(F_o^2 - F_c^2)^2]/\Sigma[w(F_o^2)^2]\}^{1/2}$ for observed data only.
(42) Ibers, J. A.; Hamilton, W. C. *Acta Crystallogr.* **1964**, *17*, 781.

Table 3. Equilibrium Study for CuX−Bpy Systems[a]

temp, °C	10 mM CuCl	10 mM CuBr	10 mM CuI
25	[Bpy] = 1.0−4.0: type **2** [Bpy] = 5.0−7.0: mixture [Bpy] = 8.0−20.0: type **1**	[Bpy] = 1.0−4.0: type **2** [Bpy] = 5.0−7.0: mixture [Bpy] = 8.0−20.0: type **1**	[Bpy] = 1.0−5.0: type **2** [Bpy] = 6.0−10.0: mixture [Bpy] = 12.0−40.0: type **1**
75	samples decomposed	[Bpy] = 1.0−3.0: type **2** [Bpy] = 4.0−6.0: mixture [Bpy] = 7.0−10.0: type **1**	[Bpy] = 1.0−10.0: type **2** [Bpy] = 12.0−14.0: mixture [Bpy] = 16.0−40.0: type **1**

[a] All concentrations in mM. Product type judged by precipitate color.

attenuation coefficients are those of Creagh and Hubbell.[44] All calculations were performed using the teXsan[45] crystallographic software package of Molecular Structure Corp.

Thermogravimetric Analysis. All TGA analyses were conducted under flowing nitrogen (20 mL/min) using a platinum pan. About 15 mg of copper(I) complex were subjected to a linear temperature ramp of 5 °C min^{-1} up to 800 °C.

Results

Synthesis of CuX−B Complexes. The addition of bridging ligand to copper(I) halide in CH_3CN solution produced solid product within a few seconds to a few minutes. In the case of CuCl− and CuBr−Quin combinations, the products were fairly soluble in CH_3CN and complete precipitation was ensured through the addition of ether. Of the B ligands shown in Chart 3, only the CuX−DMP (X = Cl, Br, I) combinations failed to produce products. A complete list of the CuX−B products prepared is shown in Table 1.

Synthesis of CuXL−B Complexes. The soluble cubane tetrameric complexes $[CuXL]_4$ (L = $P(OPh)_3$; X = Cl, Br)[9,28] proved to be useful starting materials for reactions with B. In contrast to CuCl and CuBr, CuI forms $[CuIL_2]$ as the only isolable product with L. Nevertheless, 1:1−1.5 mixtures of CuI:L were found to effect the desired reactions with B. Addition of extra L to helped to avoid traces of $[(CuX)_2B]$ contaminant in the product. Addition of B to chloroform or acetonitrile solutions of [CuXL] either directly produced yellow solids or formed yellow solutions from which product could be precipitated upon addition of ether. A list of the characterized CuXL−B products is found in Table 2.

The combinations that failed to yield products included CuIL−Quin and CuXL−Phz (X = Br, I), each of which yielded the phosphite-free type **2** product, $[(CuX)_2B]$. In these cases, the desired product apparently formed in solution. Thus, for example, when a red suspension of $[(CuI)_2(Quin)]$ in CH_3CN was treated with a ca. 5-fold excess of L, a lemon-colored solution (presumably containing $[(CuIL)_2(Quin)]$) formed. Nevertheless, only red $[(CuI)_2(Quin)]$ could be isolated upon addition of ether. The $[(CuClL)_2(Phz)]$ product was found to be at the brink of stability. In all but one attempt to synthesize this product, dark brown $[(CuCl)_2(Phz)]$ crystals were formed. However, in a single instance using CH_3CN solvent, a relatively unstable red-brown powder that analyzed fairly well for the desired product was isolated (see Table 2). The white products of the CuIL−DMP and CuIL−HMTA reactions apparently incorporate the intended components, but thus far, these species has resisted definitive characterization.

Characterization of Products. Most of the CuX−B and many of the CuXL−B products were found to be insoluble in common solvents. Nevertheless, in many cases, good quality crystals were produced by direct synthesis in acetonitrile. Due to their insolubility, the stoichiometry of the new compounds was determined primarily through elemental analyses (see Tables 1 and 2). Two ratios were encountered for the CuX−B products. Red type **1** complexes, [CuXB], were accessible for systems in which B = Bpy and Pyz (except X = I). Type **2** stoichiometry, $[(CuX)_2B]$, was more prevalent, being found for all of the CuX−B combinations, except CuCl−Pyz[46] and CuBr−Pyz, and those of DMP (which formed no phosphite-free products). Type **2** product colors varied widely, depending on the degree of conjugation of B. Complexes of nonaromatic DABCO and HMTA showed little to no color. Those having simple aromatic B ligands (Bpy and Pyz) were yellow. Those with fused ring systems were red (Quin) or dark brown (Phz). $[(CuI)_2(Phz)]$ had a very unusual appearance, being black with a gold luster.

For B = Bpy, both type **1** and **2** complexes could be synthesized for each halide through careful control of synthetic conditions. In all cases, the yellow type **2** precipitate, $[(CuX)_2(Bpy)]$, was initially produced upon combination of dilute acetonitrile solutions of CuX (10 mM) and Bpy (1−20 mM) at room temperature. When the CuX−Bpy mixtures were stirred at 25 or 75 °C in sealed vials, equilibrium 1 was established over a period of a few minutes to a few hours.

$$[(CuX)_2(Bpy)]\ (\mathbf{2}, \text{yellow}) + Bpy \rightleftharpoons 2[CuX(Bpy)]\ (\mathbf{1}, \text{red}) \quad (1)$$

The approximate position of equilibrium 1 for the two insoluble complexes was readily judged by precipitate color (Table 3). The position of equilibrium for CuCl−Bpy (25 °C) and CuBr−Bpy (25, 75 °C) were roughly identical. (Mixtures containing CuCl−Bpy decomposed at this temperature.) The 25 °C position of equilibrium 1 for CuI−Bpy lay slightly to the left than those of the other halides, and at 75 °C, the iodide equilibrium was shifted much further to the left.

Elemental analysis data confirmed a 2:1 stoichiometry for most of the CuXL−B products. X-ray crystallography of two compounds (see below) confirmed the expected type **3** polymeric structure. Only the two characterizable CuXL−HMTA combinations showed 1:1 stoichiometry. An X-ray structure (see below) unexpectedly showed a square dimer (**4**) (Chart 4). No CuXL−B combination afforded multiple stoichiometries.

X-ray Crystallography. Structural determinations were completed for several complexes that were representative of the various structural types encountered: [CuBr(Pyz)] (type **1b**); $[(CuI)_2(Quin)]$ (type **2**); $[(CuBr)_2(P(OPh)_3)_2(Bpy)]$ (type **3**); $[(CuBr)_2(P(OPh)_3)_2(Pyz)]$ (type **3**); $[(CuBr)(P(OPh)_3)(HMTA)]$ (**4**). Crystallographic data are summarized in Table 4. Selected bond lengths and angles are given in Table 5.

(43) Creagh, D. C.; McAuley, W. J. In *International Tables for Crystallography*; Wilson, A. J. C., Ed.; Kluwer Academic Publishers: Boston, MA, 1992; Vol. C, Table 4.2.6.8, pp 219−222.
(44) Creagh, D. C.; Hubbell, J. H. In *International Tables for Crystallography*; Wilson, A. J. C., Ed.; Kluwer Academic Publishers: Boston, MA, 1992; Vol. C, Table 4.2.4.3, pp 200−206.
(45) *TeXsan for Windows, Crystal Structure Analysis Package*; Molecular Structure Corp.: The Woodlands, TX, 1985, 1992.
(46) Although $[(CuCl)_2(Pyz)]$ did not form in the current study, it is known. See ref 20.

Table 4. Crystal and Structure Refinement Data[a]

	sample				
	[CuBr(Pyz)]	[(CuI)$_2$(Quin)]	[(CuBrL)$_2$(Bpy)]	[(CuBrL)$_2$(Pyz)]	[CuBrL(HMTA)]
formula	$C_4H_4BrCuN_2$	$C_8H_6N_2Cu_2I_2$	$C_{46}H_{38}Br_2Cu_2N_2O_6P_2$	$C_{40}H_{34}Br_2Cu_2N_2O_6P_2$	$C_{24}H_{27}N_4O_3PCuBr$
fw	223.54	511.03	1063.66	987.57	593.92
space group	*P*2/*c* (No. 13)	*P*2$_1$/*c* (No. 14)	*P*$\bar{1}$ (No. 2)	*P*$\bar{1}$ (No. 2)	*P*2$_1$/*c* (No. 14)
a, Å	3.986(3)	4.3718(6)	9.356(3)	8.4327(5)	12.638(2)
b, Å	6.579(5)	17.718(2)	13.298(4)	10.4990(9)	11.710(3)
c, Å	11.399(1)	14.7481(4)	9.446(3)	13.907(1)	17.3401(5)
α, deg	90	90	105.51(2)	74.083(3)	90
β, deg	96.621(3)	110.163(1)	96.29(3)	77.501(2)	103.501(1)
γ, deg	90	90	70.38(2)	62.816(1)	90
V, Å^3	296.9(3)	1072.4(1)	1066.4(6)	1047.3(1)	2495.2(5)
Z	2	4	1	1	4
ρ_{calc}, g cm^{-3}	2.500	3.165	1.656	1.566	1.581
F_{000}	212	928	534	494	1208
μ(Mo Kα), mm^{-1}	10.28	9.681	3.003	3.046	2.574
radiatn (*λ*, Å)	Mo Kα (0.710 73)	Mo Kα (0.710 73)	Mo Kα (0.710 73)	Mo Kα (0.710 73)	Mo Kα (0.710 73)
temp, °C	20	20	−100	20	20
residuals: *R*; R_w	0.049; 0.056	0.067; 0.131	0.031; 0.036	0.042; 0.047	0.111; 0.107
goodness of fit	1.113	1.318	1.29	1.186	1.051

[a] L = P(OPh)$_3$. [b] $R = R_1 = \Sigma||F_o| - |F_c||/\Sigma|F_o|$ for observed data only. $R_w = wR_2 = \{\Sigma[w(F_o^2 - F_c^2)^2]/\Sigma[w(F_o^2)^2]\}^{1/2}$ for all data. [c] $R = \Sigma||F_o| - |F_c||/\Sigma|F_o|$ for observed data only. $R_w = \{\Sigma[w(F_o^2 - F_c^2)^2]/\Sigma[w(F_o^2)^2]\}^{1/2}$ for observed data only.

Chart 4

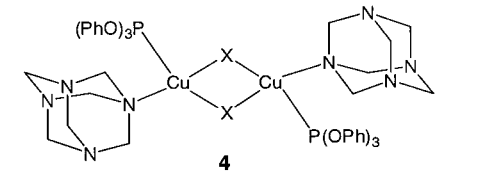

4

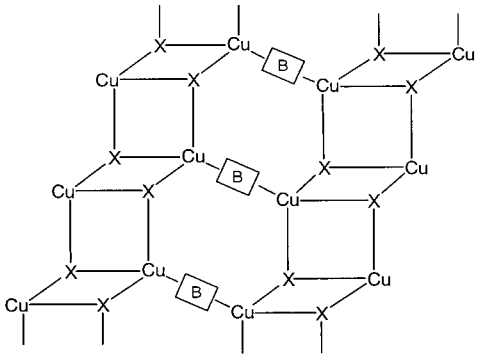

5

The sheet structure and packing arrangement for [CuBr(Pyz)] are shown in Figures 1 and 2. The structure is of type **1b** (see Chart 2). It consists of approximately tetrahedral copper atoms linked along the *c*-direction by Pyz rings and along the *a*-direction by Br atoms to form infinite 2D sheets, which stack along the *b*-axis to complete the structure. The Cu and Br atoms sit on crystallographic 2-fold axes at (0, *y*, 1/4) and (1/2, *y*, 1/4), respectively. The Pyz ring is situated about an inversion center at (0, 0, 1/2). The structure can be regarded as a series of zigzag (CuBr)$_\infty$ polymers (see Chart 1) which are cross-linked by Pyz ligands. The resulting undulating sheets are composed of fused rectangular $Cu_4Br_2(Pyz)_2$ metallocycles with Cu atoms at the corners (see Figure 2). The spacing between adjacent sheets corresponds to the *b*-cell dimension, about 6.6 Å (see Figure 3). There is a weak C−H···Br contact between adjacent stacked layers. The H(2)···Br(1) distance of 2.97(5) Å is at the limit of van der Waals contact,[47] but the C(2)−H(2)···Br(1) angle of 151(3)° is within the accepted range of angles (119.3−169.2°) for this type of interaction.[48]

The sheet structure and packing arrangement diagrams for [(CuI)$_2$(Quin)] are shown in Figures 3 and 4. The type **2** structure is composed of Cu_2I_2 dimer units linked through bridging Quin ligands to form an infinite chain which lies on the 2$_1$ screw axis (i.e. adjacent Cu_2I_2(Quin) units are related by a 2$_1$ screw operation). Chains related by translation along the *a*-axis are linked by an additional Cu−I bond at each copper center to form infinite 2D layers. The layers stack in the *c*-direction to complete the structure. *π*-Stacking of Quin ligands within layers is evidenced. Neighboring sheets are related by inversion symmetry and are separated by half the *c*-axis repeat distance (about 7.4 Å).

The molecular structure diagrams for the 1D polymers [(CuBr)$_2$(P(OPh)$_3$)$_2$(Bpy)] and [(CuBr)$_2$(P(OPh)$_3$)$_2$(Pyz)] are shown in Figures 5 and 6, respectively. A packing diagram for the Pyz complex is depicted in Figure 7. Both complexes are type **3** polymers. Each chain consists of (CuL)$_2$Br$_2$ dimers linked by B ligands. The nearly perfect tetrahedral Br−Cu−N angles (97.2−104.5°) produce roughly zigzag chains, which run parallel to the *a*-axis and pack in the *y* and *z* directions through molecular interactions to complete the structures. The bulky phosphite ligand tends to fill the space on either side of the polymer chains. Given the large size of L, the deviations from tetrahedral angles around the copper atom (aside from the characteristically acute Cu−Br−Cu angles) are relatively small.

The molecular structure diagram for [(CuBr)(P(OPh)$_3$)(HMTA)] (type **4**) is found in Figure 8. The compound is a halide-bridged dimer (see Chart 1) with monodentate HMTA ligands. No polymerization is evidenced. The rhomboid Cu_2Br_2 unit is situated about an inversion center (1/2, 1/2, 0). There are no uncharacteristically close contacts or other unusual packing features.

Thermogravimetry. All of the products were analyzed using a TGA apparatus under 20 mL min^{-1} flowing nitrogen. The temperature was ramped at a rate of 5° min^{-1} from 25 to 800 °C. Although intermediate stages of decomposition were readily assigned for most of the complexes, the final decomposition stage did not produce copper metal or other identifiable material. Typically, the final mass was between that of CuX and Cu, suggesting a probable mixture of the two. The results of TGA

(47) Rowland, R. S.; Taylor, R. *J. Phys. Chem.* **1996**, *100*, 7384.
(48) Taylor, R.; Kennard, O. *J. Am. Chem. Soc.* **1982**, *104*, 5063.

Table 5. Selected Bond Distances (Å) and Angles (deg)[a]

	[CuBr(Pyz)]	[$(CuI)_2$(Quin)][b, c]	[$(CuBrL)_2$(Bpy)]	[$(CuBrL)_2$(Pyz)]	[CuBrL(HMTA)]
Cu(1)−N(1)	2.046(4)	2.047(7)	2.037(4)	2.058(2)	2.077(3)
Cu(1)−N(1′)	2.046(4)				
Cu(1)−X(1)	2.469(2)	2.764(1)	2.4696(8)	2.4843(5)	2.5541(9)
Cu(1)−X(1′)	2.469(2)	2.628(1)	2.550(1)	2.4988(5)	2.4827(8)
Cu(1)−X(2)		2.677(1)			
Cu(1)−P(1)			2.173(1)	2.1604(8)	2.157(1)
(1)−Cu(1)−X(1′)	107.65(7)	108.32(5)	105.68(3)	106.71(2)	102.42(3)
X(1)−Cu(1)−X(2)		97.98(4)			
X(1)−Cu(1)−N(1)	105.2(1)	108.3(2)	104.5(1)	103.41(7)	101.7(1)
X(1)−Cu(1)−N(1′)	113.7(1)				
X(1′)−Cu(1)−N(1)	113.7(1)	111.8(2)	97.2(1)	99.70(7)	99.2(1)
X(1)−Cu(1)−N(1′)	105.2(1)				
X(2)−Cu(1)−N(1)		110.8(2)			
X(2)−Cu(1)−X(1′)		118.31(5)			
N(1)−Cu(1)−N(1′)	111.5(3)				
P(1)−Cu(1)−X(1)			118.75(5)	118.63(3)	105.04(4)
P(1)−Cu(1)−X(1′)			109.55(5)	111.52(3)	116.74(4)
P(1)−Cu(1)−N(1)			118.4(1)	115.20(7)	128.2(1)
Cu(1)−X(1−Cu(1′)	107.65(7)	108.32(5)	74.32(3)	73.29(2)	77.58(3)
Cu(1)−X(1)−Cu(2)		79.78(4)			
Cu(2)−X(1)−Cu(1′)		63.11(4)			

[a] L = $P(OPh)_3$; X = Br or I. [b]Additional bond lengths for [$(CuI)_2$(Quin)]: Cu(2)−I(1) 2.701(1), Cu(2)−I(2) 2.657(1), Cu(2)−I(2′) 2.678(1), Cu(2)−N(2′) 2.054(7). [c]Additional bond angles for [$(CuI)_2$(Quin)]: I(1)−Cu(2)−I(2) 100.06(4), I(1)−Cu(2)−I(2′) 115.73(4), I(1)−Cu(2)−N(2′) 121.5(2), I(2)−Cu(2)−I(2′) 110.07(5), I(2)−Cu(2)−N(2′) 107.8(2), I(2′)−Cu(2)−N(2′) 101.4(2), Cu(1)−I(2)−Cu(2) 82.17(4), Cu(1)−I(2)−Cu(2′) 62.79(4), Cu(2)−I(2)−Cu(2′) 110.07(5).

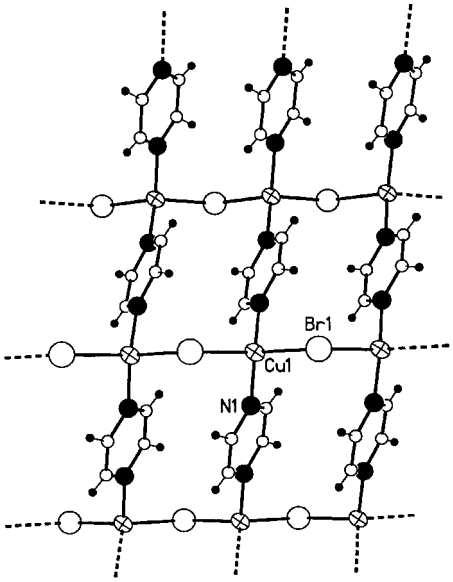

Figure 1. Sheet arrangement of [CuBr(Pyz)].

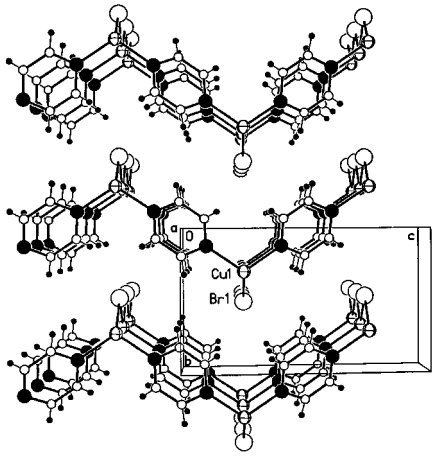

Figure 2. Packing diagram for [CuBr(Pyz)].

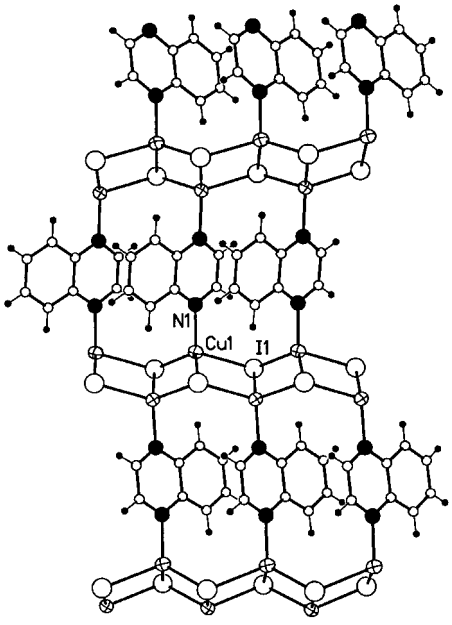

Figure 3. Sheet arrangement of [$(CuI)_2$(Quin)].

for complexes without L are provided in Table 6, and several representative TGA traces are shown in Figures 9 and 10. Complexes of type **1** (CuXB) each showed an initial mass loss corresponding to loss of 0.5 equiv of B ligand. This loss began at about 110−210 °C and resulted in a stoichiometry ($CuXB_{1/2}$) identical to that of the type **2** complexes. The next stage of decomposition for [CuX(Bpy)] (X = Cl, Br), commencing at 250−300 °C, produced the new phase $(CuX)_2B_{1/2}$. The last interpretable stage decomposition for all type **1** Bpy (beginning 320−410 °C) and Pyz (beginning at 190−260 °C) complexes produced CuX. The overall sequence for the type **1** complexes is illustrated by reactions 2 and 3.

$$\text{CuXB (}\mathbf{1}\text{)} \rightarrow 1/2(\text{CuX})_2\text{B (}\mathbf{2}\text{)} \quad (2)$$

$$(\text{CuX})_2\text{B (}\mathbf{2}\text{) (}\rightarrow(\text{CuX})_2\text{B}_{1/2}\text{)} \rightarrow 2\text{CuX} \quad (3)$$

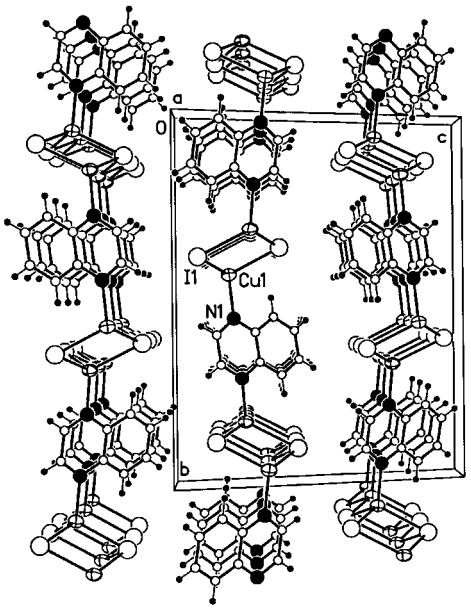

Figure 4. Packing diagram for $[(CuI)_2(Quin)]$.

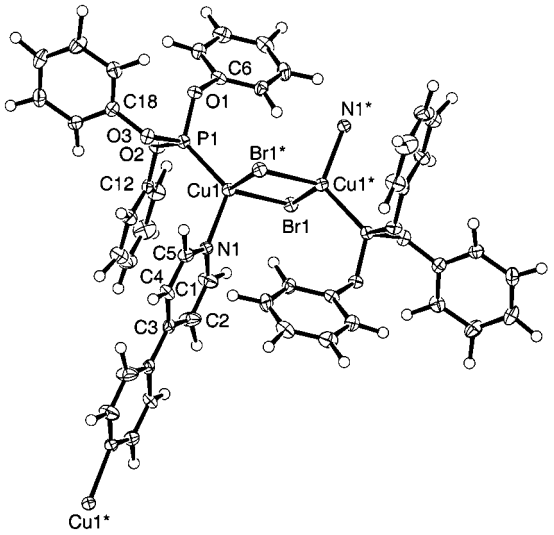

Figure 5. Molecular structure of $[(CuBr)_2(P(OPh)_3)_2(Bpy)]$.

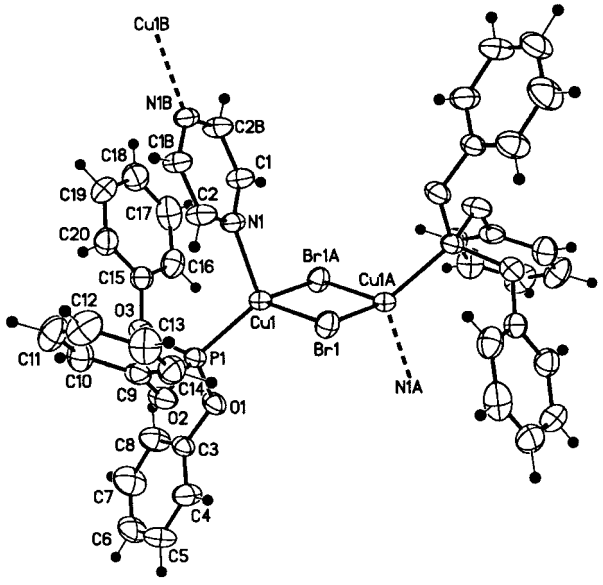

Figure 6. Molecular structure of $[(CuBr)_2(P(OPh)_3)_2(Pyz)]$.

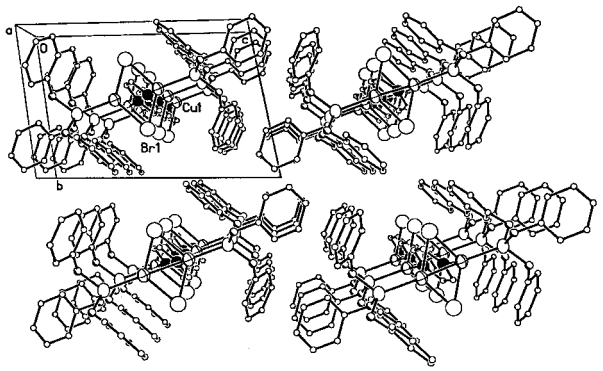

Figure 7. Packing arrangement of $[(CuBr)_2(P(OPh)_3)_2(Pyz)]$. Hydrogen atoms omitted for clarity.

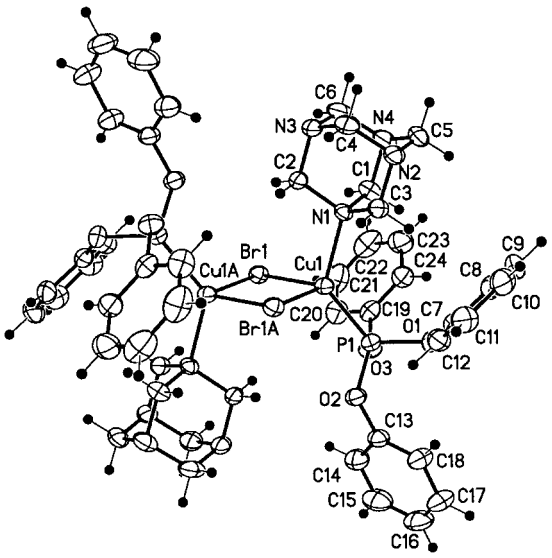

Figure 8. Molecular structure of $[(CuBr)(P(OPh)_3)(HMTA)]_2$.

The TGA results for most of the type **2** complexes suggested decomposition steps corresponding to the later stages of the type **1** sequence (reaction 3). As a result, the type **2** species required higher temperatures to initiate decomposition. Consistent with the assignments in reactions 2 and 3, TGA results of $[(CuX)_2(Bpy)]$ (X = Cl, Br, I) were roughly identical to those of [CuX(Bpy)] (following the initial conversion **1** → **2**). The type **2** complexes of Pyz, Quin, and Phz decomposed directly to CuX, beginning 160−260 °C, as shown in reaction 3. Type **2** complexes $[(CuCl)_2(Quin)]$ and $[(CuX)_2(HMTA)]$ (X = Cl, Br) each passed through an intermediate $(CuX)_2B_{1/2}$ stage, as was found for several of the type **1** species. The TGA behavior of the DABCO and HMTA complexes was more complicated and initiated at relatively low temperatures.

Thermogravimetric results for the complexes bearing L are less easily interpreted. The data are summarized in Table 7, and some traces are shown in Figure 11. Several distinct decomposition patterns are suggested by the data for type **3** complexes, $[(CuXL)_2B]$. These are summarized in reactions 4−7.

$$(CuXL)_2B \rightarrow (CuX)_2L \rightarrow (CuX)_2L_{1/2} \quad (4)$$

$$(CuXL)_2B \rightarrow (CuX)_2B\ (\rightarrow 2CuX) \quad (5)$$

$$(CuXL)_2B \rightarrow (CuX)_2L_{1/2}B\ (\rightarrow 2(CuX)_2B) \quad (6)$$

$$(CuXL)_2B \rightarrow 2(CuXL)_2\ (\rightarrow 2CuX) \quad (7)$$

No overall pattern, suggestive of greater lability of either B or

Table 6. Thermogravimetric Decomposition Results for [(CuX)B] and [(CuX)$_2$B] Complexes

complex	temp °C	product	wt % (theory)	wt % (actual)
[CuCl(Bpy)]	130−250	[(CuCl)$_2$(Bpy)]	67	68
[(CuCl)$_2$(Bpy)]	220−385	[(CuCl)$_2$(Bpy)$_{1/2}$]	78	83
	300−360[a]		52[a]	53[a]
	385−540	CuCl	56	59
	360−500[a]		37[a]	39[a]
[CuBr(Bpy)]	215−300	[(CuBr)$_2$(Bpy)]	74	72
[(CuBr)$_2$(Bpy)]	285−365	[(CuBr)$_2$(Bpy)$_{1/2}$]	82	81
	350−410[a]		61[a]	57[a]
[CuI(Bpy)]	200−255	[(CuI)$_2$(Bpy)]	78	77
[(CuI)$_2$(Bpy)]	285−405	CuI	71	72
	315−385[a]		55[a]	56
[CuCl(Pyz)]	125−190	[(CuCl)$_2$(Pyz)]	78	78
	200−260	CuCl	55	55
[CuBr(Pyz)]	120−165	[(CuBr)$_2$(Pyz)]	82	83
	195−255	CuBr	64	65
[(CuI)$_2$(Pyz)]	165−255	CuI	83	83
[(CuCl)$_2$(Quin)]	115−165	[(CuCl)$_2$(Quin)$_{1/2}$]	80	87
	205−250	CuCl	60	60
[(CuBr)$_2$(Quin)]	200−280	CuBr	69	71
[(CuI)$_2$(Quin)]	205−270	CuI	75	75
[(CuCl)$_2$(Phz)]	240−340	CuCl	52	54
[(CuBr)$_2$(Phz)]	260−325	CuBr	61	66
[(CuI)$_2$(Phz)]	220−270	CuI	68	68
[(CuCl)$_2$(DABCO)]	25−300[b]	CuCl	64	63
[(CuBr)$_2$(DABCO)]	25−355[b]	CuBr	72	68
[(CuI)$_2$(DABCO)]	105−325[b]	CuI	77	76
[(CuCl)$_2$(HMTA)]	180−215	[(CuCl)$_2$(HMTA)$_{1/2}$]	79	81
[(CuBr)$_2$(HMTA)]	130−245	[(CuBr)$_2$(HMTA)$_{1/2}$]	84	85
[(CuI)$_2$(HMTA)]	225−340	CuI	73	76

[a] These entries represent the continuation of the [CuX(Bpy)] decomposition. [b]Multiple decomposition steps occurring.

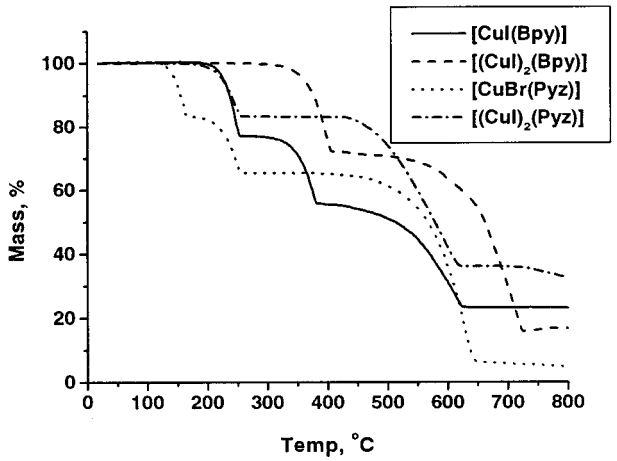

Figure 9. Thermogravimetric mass loss profiles of selected type **1** and **2** complexes.

L, is evident. The various pathways proposed involve initial release of B, L, or both. For Pyz and Quin complexes, initial loss of L (reactions 5 and 6) implies moderate stability of the Cu−B. However, early loss of B (reaction 7) occurs for B = DMP. Reaction 4 requires simultaneous initial loss of L and B. It occurs with [(CuXL)$_2$(Bpy)] (X = Cl, Br). The 1:1 complexes, [CuXL(HMTA)]$_2$ (X = Cl, Br) showed initial loss of HMTA, reaction 8.

$$[\mathrm{CuXLB}]_2 \rightarrow 2\mathrm{CuXL} \qquad (8)$$

Discussion

The copper(I) compounds CuX and [CuXL] (X = Cl, Br, I; L = P(OPh)$_3$) readily form 2:1, and occasionally 1:1, complexes

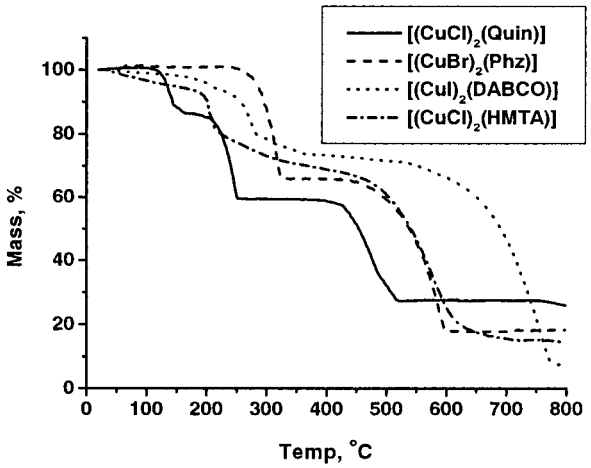

Figure 10. Thermogravimetric mass loss profiles of selected type **2** complexes.

Table 7. Thermogravimetric Decomposition Results for [(CuXL)$_2$B] and [(CuXL)B]$_2$ Complexes[a]

complex	temp, °C	product	wt % (theory)	wt % (actual)
[(CuClL)$_2$(Bpy)]	155−235	[(CuCl)$_2$L]	52	52
	290−375	[(CuCl)$_2$L$_{1/2}$]	36	40
[(CuBrL)$_2$(Bpy)]	170−240	[(CuBr)$_2$L]	56	57
	335−420	[(CuCl)$_2$L$_{1/2}$]	43	42
[(CuIL)$_2$(Bpy)]	120−275	[(CuI)$_2$(Bpy)]	46	48
	320−385	CuI	33	35
[(CuClL)$_2$(Pyz)]	105−265	[(CuCl)$_2$L$_{1/2}$(Pyz)]	48	46
	410−515	[(CuCl)$_2$(Pyz)]	31	30
[(CuBrL)$_2$(Pyz)]	140−300	[(CuBr)$_2$(Pyz)]	37	40
[(CuIL)$_2$(Pyz)]	130−240	[(CuI)$_2$(Pyz)]	46	43
[(CuClL)$_2$(Quin)]	130−305	[(CuCl)$_2$L$_{1/2}$(Quin)]	51	50
	205−250	[(CuCl)$_2$(Quin)]	35	31
[(CuBrL)$_2$(Quin)]	25−150	[(CuBr)$_2$L$_{1/2}$(Quin)]	55	55
[(CuIL)$_2$(Quin)]	50−185	[(CuI)$_2$L$_{1/2}$(Quin)]	59	60
[(CuClL)$_2$(DABCO)]	50−190	[CuClL]	88	90
	190−325	CuCl?	21	27
[(CuBrL)$_2$(DABCO)]	180−390[b]	[(CuBr)$_2$(DABCO)]	39	39
	455−575	CuBr?	28	21
[(CuIL)$_2$(DABCO)]	135−230	[(CuI)$_2$L$_{1/2}$(DABCO)]	58	56
	315−460	[(CuI)$_2$(DABCO)]	44	44
[(CuClL)$_2$(DMP)]	135−170	[CuClL]	88	92
	170−320	CuCl?	21	27
[(CuBrL)$_2$(DMP)]	135−185	[CuBrL]	89	88
	185−245	CuBr?	29	36
[(CuIL)$_2$(DMP)]	70−115	[CuIL]?	81	95
	115−260	CuI?	31	36
[CuClL(HMTA)]$_2$	155−210	[CuClL]	75	76
[CuBrL(HMTA)]$_2$	155−220	[CuBrL]	76	73

[a] L = P(OPh)$_3$. [b]Multiple decomposition steps occurring.

with the B ligands shown in Chart 3, with only a few exceptions. When B is aromatic, colored products are obtained. The origin of this color is almost certainly metal-to-ligand charge transfer (MLCT). Since MLCT can occur only for unsaturated bridging ligands (which have π^* orbitals), the complexes of saturated B ligands, DABCO, HMTA, and DMP, were found to be white or off-white. Also consistent with MLCT, the stabilization of the π^* orbitals in fused-ring polycyclic aromatic systems results in shifts from yellow to red absorption colors. The complexes that incorporate L are less intensely colored than those without L. Moreover, the addition of L tends to produce yellow color, rather than orange or red, presumably as a result of the displacement of the MLCT absorption band to higher energy.

Structural determinations have revealed that four of the new complexes contain the well-known cyclic Cu_2X_2 units. The preference for these units is probably due, at least in part, to

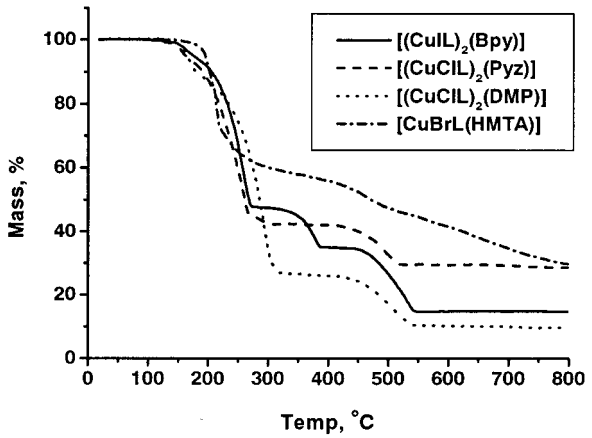

Figure 11. Thermogravimetric mass loss profiles of selected type **3** and **4** complexes.

the acute Cu−X−Cu angles formed, which allow greater room for other ligands. The new type **2** and **3** complexes form polymeric chains through the linking of Cu_2X_2 units. The type **3** polymer strands of $[(CuBr)_2(P(OPh)_3)_2(Bpy)]$ and $[(CuBr)_2(P(OPh)_3)_2(Pyz)]$ are widely separated, due to the bulky L groups, which flank each chain. The choice of the larger Bpy or the smaller Pyz appears to exert no significant influence on the structure. Similar type **3** polymers are formed for these B ligands with L = PPh_3.[5,23,24] In the type **2** complex, $[(CuI)_2(Quin)]$, the Cu_2I_2 units are connected in a stair step fashion to form $[Cu_2I_2]_\infty$ chains. The chains are linked into layers through Quin bridging. Unlike the sheets of the [CuBr(Pyz)] which are formed from zigzag chains, sheets in the Cu−Quin structure show relatively little "rippling". The structure bears a close analogy to those of $[(CuX)_2(Phz)]$ (X = Cl, Br)[19] and $[(CuCl)_2(Pyz)]$.[20] Prior to the current work, only one crystal structure of a Cu(I)−quinoxaline complex, $[Cu_2(\mu\text{-}ClO_4)(Quin)_3]ClO_4$, was known.[49]

The atom arrangement in [CuBr(Pyz)] does not correspond to the type **1a** structure exhibited by [CuCl(Bpy)][14] or [CuBr(3,4′-Bpy)],[15] which is based upon linked Cu_2X_2 units. Instead, $(CuX)_\infty$ chains are present forming a gridlike type **1b** pattern. Similar structures have been encountered for [CuY(Pyz)] (Y = Cl, μ-1,3-SCN, μ-1,3-N_3, μ-1,1-OCN)[18,22,24] and for [CuBr(cnge)].[17] Presumably, it is the size differential in B that is responsible for the formation of type **1b** structures for Pyz and type **1a** for Bpy.

The "type **4**" structure was found to be that of a simple dimer, based on Cu_2Br_2 (see Chart 1). Halide-bridged dimers are routinely encountered when monodentate ligands are bound to CuX.[8] As with the type **3** polymers, the Cu_2Br_2 unit is coordinated by both L and B. However, instead of incorporation of a half unit of bridging B, which would allow for polymerization, a full equivalent of monodentate B is present. Presumably, the combination of bulky L and B ligands interferes with chain formation. A single-crystal structure of Cu(I)−HMTA, that of $[(CuCN)_3(HMTA)_2]$, has been previously reported;[50] it showed bidentate bridging HMTA.

Thermal analysis of the CuX−B complexes uncovered a series of steps comprising the loss of B. This sequence, shown in eqs 2 and 3, reveals three distinct CuX:B ratios: 1:1, 2:1, and 4:1. However, only the former two ratios represent isolable stoichiometries: types **1** and **2**, respectively. The 4:1 complex, $[(CuX)_2B_{1/2}]$, was identified from TGA data during the decomposition of [CuX(Bpy)]/$[(CuX)_2(Bpy)]$ (X = Cl, Br), $[(CuCl)_2(Quin)]$, and $[(CuX)_2(HMTA)]$ (X = Cl, Br). It appears to be metastable, since efforts to prepare the 4:1 complex have proved unsuccessful. To our knowledge, the only precedent for this highly ligand-deficient stoichiometry in the complexes of CuX is the hydrothermally synthesized $[(CuCN)_4(Biquin)]$, (Biquin = 2,2′-biquinoline), which contains both three- and two-coordinate copper sites.[25a] In the present case, the use of a bridging B, rather than chelating Biquin, and the use of halide, rather than CN, probably allows for a more highly networked structure. We suggest structure **5** (Chart 4), based upon the ubiquitous Cu_2X_2 framework. This infinite step polymer features only three-coordinate copper. Step type tetramers of CuX exhibiting both three- and even two-coordinate Cu centers are known.[8b,13a,51]

It is noteworthy that two separate stoichiometric ratios can be formed in several cases, notably: CuX−Bpy. Although there are literature reports of both types **1** and **2** for CuCl−Pyz,[18,20] $[(CuCl)_2(Pyz)]$ was prepared serendipitously and could not be formed through direct synthesis in the current study. The coexistence of types **1** and **2** complexes for Bpy (and possibly Pyz) suggests similar thermal stability of these phases. The TGA data reveal that, for type **1** complexes, the first decomposition step invariably is **1** → **2**. This could be interpreted as indicating greater thermal stability of **2**. However, due to the flowing N_2 gas used in the TGA work, the results do not necessarily reflect equilibrium conditions, since the liberated B ligand is swept away in the vapor phase. As a result, TGA data are expected to favor complexes that are deficient in volatile ligands.

The preliminary study of equilibrium 1 revealed several features of note: At the concentrations used, the type **2** complex was found to be the kinetic product for all three CuX−Bpy systems (regardless of ratio or mixing sequence). The thermodynamic stabilities of the type **1** and **2** complexes appear to be similar for CuCl− and CuBr−Bpy (see Table 3). However, the type **2** product for CuI−Bpy appeared to have a larger region of stability. The foregoing implies that CuI complexation differs from that of CuCl and CuBr; this was further supported by other observations: $[(CuX)_2(Pyz)]$ readily forms only in the case of the iodide. Three ligand combinations (CuXL−Quin, CuXL−DMP, and CuXL−HMTA) proved successful for CuCl and CuBr but not for CuI. These differences may reflect a greater tendency of CuI complexes to adopt three-coordination. Such was found to be the case with the type **2** series $[(CuX)_2(Phz)]$,[19] in which only the iodide lacked cross-linking (dashed lines in Chart 2).

Finally, it was noted that the new network complexes of copper, especially those containing the phosphite, are not especially thermally robust. This reduced stability probably reflects not only the lability of L, but also the lesser degree of networking, due to the replacement of B with L. It was also apparent that the unsaturated B ligands generally formed more thermally stable complexes. This fact is probably due to d−π* bonding, which is favored by electron-rich metal centers such as Cu(I).

Conclusions

A wide array of CuX−B and CuXL−B complexes have been prepared. The former combination produces both [CuXB] and $[(CuX)_2B]$ networks. Both ratios are readily accessible when B

(49) Lumme, P.; Lindroos, S.; Lindell, E. *Acta Crystallogr., Sect. C* **1987**, *43*, 2053.
(50) Stocker, F. B. *Inorg. Chem.* **1991**, *30*, 1472.
(51) Churchill, M. R.; Kalra, K. L. *Inorg. Chem.* **1974**, *13*, 1427. (b) Churchill, M. R.; DeBoer, B. G.; Donovan, D. J. *Inorg. Chem.* **1975**, *14*, 617.

= Bpy. Most of the phosphite-containing products have the $[(CuXL)_2B]$ formulation. Structural studies have shown that the networks produced are two-dimensional in the case of CuX−B and one-dimensional, or even nonpolymeric, for CuXL−B. Thermal analyses of the phosphite-free complexes support the general trend: **1** → **2** → $[(CuX)_2B_{1/2}]$ → CuX. The complexes containing $P(OPh)_3$ were generally less thermally stable and were found to decompose by a variety of pathways.

Acknowledgment. Acknowledgment is made to the Petroleum Research Fund of the American Chemical Society (Grant No. PRF 32226-B3), to the Camille and Henry Dreyfus Foundation (Grant No. TH-99-010), and to the Thomas F. and Kate Miller Jeffress Memorial Trust (Grant No. J-440) for support of this research.

Supporting Information Available: Complete crystallographic data in CIF format and molecular diagrams for [CuBr(Pyz)] and $[(CuI)_2$(Quin)]. This material is available free of charge via the Internet at http://pubs.acs.org.

IC0005341